

Generator–Refiner–Examiner: A Tri-Module Data Augmentation Framework for 3D Human Avatar Learning from Monocular Videos

Gangjian Zhang
HKUST(GZ)
Guangzhou, China

Jian Shu
HKUST(GZ)
Guangzhou, China

Sicheng Yu
HKUST(GZ)
Guangzhou, China

Wenhao Shen
Nanyang Technological University
Singapore

Yu Feng
HKUST(GZ)
Guangzhou, China

Hao Wang*
HKUST(GZ)
Guangzhou, China



Figure 1: Qualitative Comparison. We use the same SMPL templates to drive the animatable 3D avatars of different SOTA methods and render 2D images. In comparison, our method achieves more accurate reconstruction of clothing wrinkles, smoother clothing connections, and fewer visual artifacts. Please refer to the supplementary material for more video demos.

Abstract

This paper addresses the challenge of reconstructing photorealistic and animatable 3D human avatars from monocular videos. While existing methods rely on combining per-subject optimization with generic human priors, they often fail to capture fine-grained details when training frames are limited. To mitigate this data scarcity, we propose TrioMan, a systematic tri-module framework for augmented 3D avatar learning. Our approach comprises three synergistic components. The Generator creates diverse unseen samples by imposing Gaussian perturbations on pose and camera. The Refiner improves the quality of generated data through one-step diffusion guided by texture and geometry cues. The Examiner selects subject-consistent samples using a dual-branch attention-based similarity evaluation. Experiments on the X-Humans and NeuMan benchmarks show that TrioMan outperforms state-of-the-art methods.

*Corresponding author.

Email: {gzhang292, haowang}@connect.hkust-gz.edu.cn
Demo page: <https://gre2026.github.io/GRE2026/>

1 Introduction

Photorealistic, animatable 3D avatars are essential for immersive technologies like VR and AR. Reconstructing high-fidelity avatars from monocular videos is a key goal, as it alleviates the need for costly multi-view capture systems [1, 3] or 3D scans. Recent progress in 3D Gaussian Splatting (3DGS) [23] has boosted avatar reconstruction from monocular input [9, 12, 14, 38].

However, monocular video-based reconstruction [9, 10, 12, 14, 19, 21, 38, 43, 44, 61] still suffers from limited input diversity and insufficient viewpoint coverage. A typical monocular video [21, 51] lasts less than a minute, capturing only a small set of poses and camera angles. This narrow range restricts the model’s ability to reconstruct consistent geometry and appearance under unseen motions or views.

To improve reconstruction performance under limited data, recent works such as PGHM [43] and Vid2Avatar-Pro [10] introduce prior knowledge. The former uses multi-view human datasets [5, 65] to train parametric priors that regularize reconstruction and reduce

overfitting. The latter learns a universal prior from 1,000 in-the-wild performances and fine-tunes it on the target subject. While these priors improve pose generalization, they focus on generic human characteristics than more pertinent subject-specific details. As a result, they struggle to directly address the fundamental limitation of capturing personalized dynamics from monocular input.

Toward this end, this paper introduces TrioMan, a tri-module augmented avatar learning framework designed to enrich training diversity, enhance synthetic-real consistency, and ensure sample reliability. Built upon 3DGS [23] and SMPL-X [42] modeling, TrioMan features three tightly coupled modules: the Generator, Refiner, and Examiner.

Collectively, these components address the challenge of limited frame data in monocular video setups, without compromising the fine-grained, subject-specific details vital for realistic avatar reconstruction.

To be specific, (1) the Generator synthesizes diverse unseen training frames by sampling pose and camera perturbations from Gaussian distributions. It improves the data abundance beyond the range of the original video, addressing the limitation of training data scarcity. (2) The Refiner uses one-step diffusion [64, 70] with texture and geometry conditioning to enhance the Generator’s coarse frames into photorealistic images. It improves the consistency between synthetic and real samples. (3) The Examiner acts as a quality gatekeeper, evaluating the similarity between refined frames and real video frames using a dual-branch attention-based network. It ensures that only high-fidelity, subject-consistent pseudo samples are used for training. By integrating these three modules, TrioMan equips the model with rich and realistic training samples, covering novel human poses and camera views.

Experiments on benchmark datasets (X-Humans, NeuMan) validate that our proposed method achieves SOTA performance. Our main contributions are threefold:

- We propose a tri-module augmented avatar learning framework that systematically addresses monocular data scarcity by integrating data synthesis, synthetic-real alignment, and quality control in a unified pipeline.
- We design a distribution-perturbed Generator and a one-step diffusion Refiner, which work collectively to produce diverse, photorealistic training samples while retaining subject-specific characteristics.
- We introduce a dual-branch attention-based Examiner that mitigates the stochasticity of diffusion-based generation and provides reliable pseudo-GT for model training.

2 Related Work

2.1 Monocular Video Human Reconstruction

Reconstructing 3D human avatars from monocular videos is a critical task in computer vision, with applications in VR/AR and more. The rise of Neural Radiance Fields (NeRF) [37] enabled implicit articulated avatar reconstruction from monocular video [8, 9, 18, 19, 21, 54, 55, 57, 62, 73]. Recent advances have shifted to 3D Gaussian Splatting (3DGS) [23] for faster rendering and simpler optimization [27, 29, 49, 56]. Two paradigms have emerged: direct per-subject Gaussian parameter optimization [27, 29] and neural network-based attribute prediction [12, 15, 16, 24, 28, 34, 44, 60].

GaussianAvatar [15] uses SMPL’s UV map for pose-dependent effects, while ExAvatar [39] integrates SMPL-X for whole-body (face/hand) control. EVA [12] enhances avatar expressiveness in detailed areas through an SMPL-X alignment module and adaptive density control. More recently, Vid2Avatar-Pro [10] creates high-quality animatable avatars from monocular videos using a universal prior and diffusion-based texture inpainting. PGHM [43] combines parametric human priors with 3D Gaussian Splatting for fast and high-fidelity avatar reconstruction. PriorAvatar [20] utilizes a multi-person feature codebook as a 3D human prior to guide Gaussian-based avatar fitting. MonoCloth [22] employs a part-based decomposition strategy and a cloth simulation module to improve reconstruction and animation realism.

2.2 3DGS for Human Representation

The efficiency and high quality of 3DGS have led to its rapid adoption for realistic human avatar representation. Early works [35, 40, 53] established frameworks that map canonical Gaussians to target poses via deformation models, while hybrid representations [38, 50], where Gaussians are explicitly embedded onto a deformable mesh for enhanced structural fidelity, have been developed. Beyond subject-specific reconstruction, other research has further leveraged 3DGS for efficient text-driven 3D human generation through structure-aware sampling [25, 35, 77]. Recently, large Gaussian models for human avatar reconstruction have been widely explored and have demonstrated outstanding texture details [45, 46, 52, 69, 74, 75], enabling the synthesis of Gaussians in a feed-forward approach.

2.3 3DGS for Scene Representation

Extending 3DGS to dynamic scenes has attracted significant attention [17, 30, 71]. Mainstream approaches often involve learning complex deformation fields [63, 67] or directly optimizing Gaussian attributes across time [4, 7, 68]. While recent methods combining tri-plane and hash-coding [66] or spline functions [41] show impressive results, they often lack smoothness or require massive priors, such as 2D trajectories and depth estimation. However, these methods typically assume dense multi-view supervision or known camera poses, which are unavailable in monocular videos. Furthermore, they rarely model articulated human topology, leading to distorted limbs during fast motion. While recent works [32, 33, 64, 72, 78] leverage generative priors, like diffusion models, to refine details or regularize reconstructions from sparse inputs, their application is limited to static refinement and does not address the core data scarcity of novel poses and viewpoints in monocular human video.

3 Methodology

3.1 Preliminaries

Gaussian Splatting. Gaussian splatting [23], emerging as a popular 3D representation, utilize a collection of 3D Gaussians, denoted by \mathcal{G} , to model 3D data. Each 3D Gaussian is characterized by a parameter set: $\{\mathbf{x}_i, \mathbf{s}_i, \mathbf{q}_i, \alpha_i, \mathbf{c}_i\} \in \mathbb{R}^{14}$. Here, $\mathbf{x} \in \mathbb{R}^3$ represents the geometry center, $\mathbf{s} \in \mathbb{R}^3$ the scaling factor, $\mathbf{q} \in \mathbb{R}^4$ the rotation quaternion, $\alpha \in \mathbb{R}$ the opacity value, and $\mathbf{c} \in \mathbb{R}^3$ the color feature.

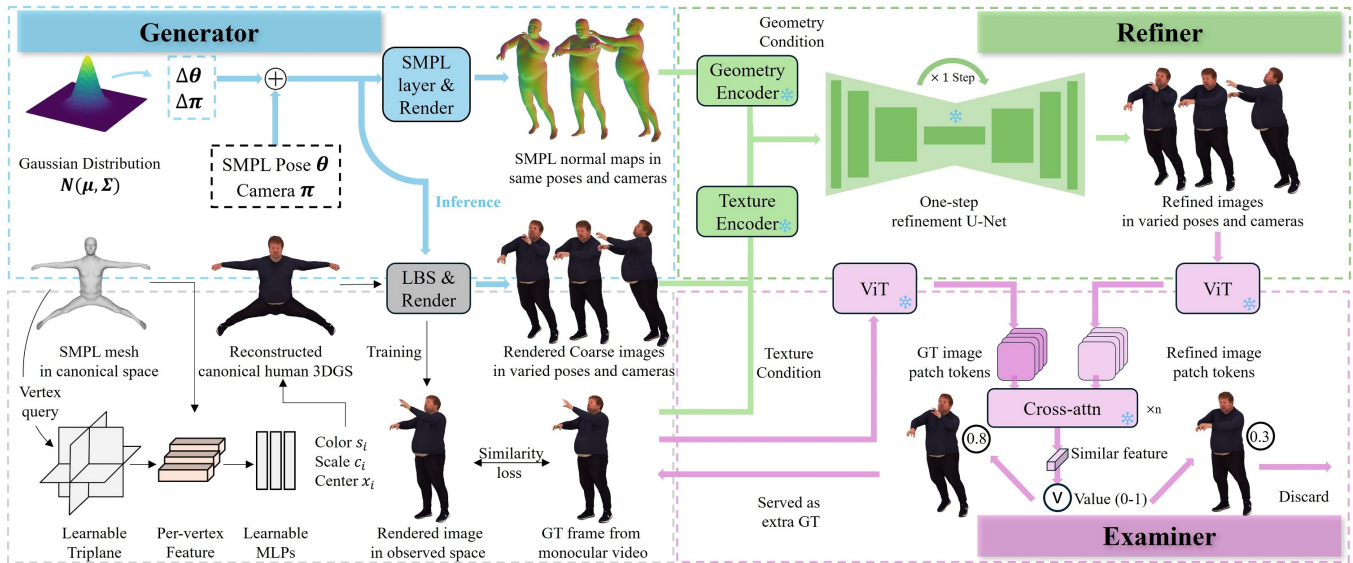


Figure 2: Method Overview. Our method, TrioMan, addresses expressive 3D human avatar learning from monocular video by introducing a tri-module (Generator-Refiner-Examiner) augmented avatar learning framework. The Generator leverages Gaussian distributions to sample pose and camera perturbations, which are fused with the SMPL pose (fitted from the video frame) and camera pose to generate SMPL pose variations that can drive the Human 3D Gaussian reconstructed from the baseline model to produce unseen coarse frames. The Refiner takes geometric conditions from variation SMPLs and texture conditions from the real frame, refining them via a one-step diffusion process to generate photorealistic refined frames. Moreover, the Examiner assesses the similarity in details between the refined frame and the real video frame to determine whether the refined frame will be included as a pseudo ground truth (GT) for the avatar learning.

SMPL(X) & LBS. Skinned Multi-Person Linear (SMPL) model [36] is a parametric human body model that generates 3D meshes by linearly blending shape and pose variations. It maps low-dimensional body parameters (Shape β and Pose θ) to 3D mesh, facilitating efficient reconstruction and animation. The human body mesh \mathcal{M} is defined as: $\mathcal{M}(\beta, \theta) : (\beta, \theta) \Rightarrow \mathbb{R}^{3 \times 6890}$. Extensions like SMPL-X [42, 47] enhance control over facial expressions, body movements.

Linear Blend Skinning (LBS) is a mesh deformation method used in models like SMPL, deforming the template mesh using parameters (θ) for body articulation.

Diffusion Model (DM). DM [11, 31, 48] learns to model the data distribution $p_{\text{data}}(\mathbf{x})$ through iterative denoising and are trained with denoising score matching. Specifically, to train a diffusion model, diffused versions $\mathbf{x}_\tau = \mathbf{x} + \sigma_\tau \epsilon$ of the data $\mathbf{x} \sim p_{\text{data}}$ are generated, by progressively adding Gaussian noise $\epsilon \sim \mathcal{N}(\mathbf{0}, \mathbf{I})$. Learnable parameters θ' of the denoiser model $\mathbf{F}_{\theta'}$ are optimized via the objective:

$$\mathbb{E}_{\mathbf{x} \sim p_{\text{data}}, \tau \sim p_\tau, \epsilon \sim \mathcal{N}(\mathbf{0}, \mathbf{I})} [\|\mathbf{y} - \mathbf{F}_{\theta'}(\mathbf{x}_\tau; \mathbf{c}, \tau)\|_2^2], \quad (1)$$

where \mathbf{c} is condition. The target vector \mathbf{y} is usually set as the added noise ϵ . Finally, p_τ denotes a uniform distribution over the diffusion time variable τ .

3.2 The Proposed Method

3.2.1 Overview. Our method, TrioMan, outlined in Figure 2, enhances the learning of expressive 3D human avatars from monocular RGB videos through a tri-module data augmentation framework.

We begin with the baseline model to reconstruct 3D human Gaussians from RGB frames (see Section 3.2.2). The Generator module then creates unseen pose and camera variations by sampling Gaussian perturbations, producing coarse images (refer to Section 3.2.3). Using this curated training data (introduced in Section 3.2.4), the Refiner module transforms these coarse images into photorealistic representations, with details in Section 3.2.5. Finally, the Examiner evaluates the refined images to identify high-quality pseudo GTs, as described in Section 3.2.6.

3.2.2 Baseline Method. Our baseline model is primarily based on ExAvatar [38], with specific operations illustrated in the lower left corner of Figure 2. It employs a typical framework for learning 3D human avatars from monocular video, using a trainable triplane to capture geometric features. These features are queried at each vertex of a canonical SMPL mesh and fed into learnable MLPs to predict attributes of Gaussian points, thereby creating canonical 3D human Gaussians. To train the triplane and MLPs, these 3D Gaussian points are bonded to the vertices of the canonical SMPL mesh, and LBS is utilized to map Gaussian points into the observation space. Concretely, a matrix transformation is then applied to these space points based on the fitted SMPL pose θ derived from a video frame, followed by 3D Gaussian rendering under the camera pose π that matches the frame view. The video frame serves as the GT for similarity calculations with the rendered image, providing supervision for gradients.

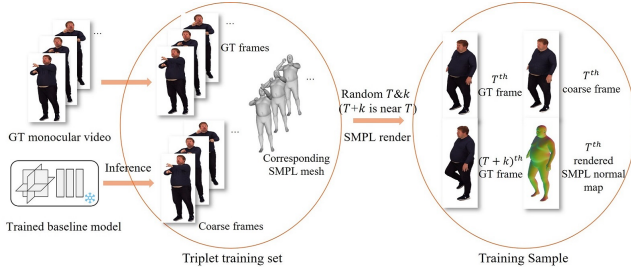


Figure 3: Data construction for Refiner and Examiner. We infer coarse frames from the trained baseline model using all the SMPL and camera parameters corresponding to GT frames in the monocular video. Along with the SMPL meshes mapped from the SMPL parameters, we compose a triplet set. We extract the GT and coarse frames at time T and render the SMPL normal map, along with the GT frame at time $T + k$, to form a training sample.

3.2.3 Generator. While the baseline model successfully reconstructs 3D human Gaussians from RGB frames, it struggles with the limited diversity of the training data, as monocular videos capture a narrow range of movements and views. To tackle this, the Generator synthesizes diverse unseen images by expanding the distribution of pose and camera parameters beyond the original video. It uses Gaussian distributions to sample perturbations, driving the baseline-reconstructed 3D Gaussians to generate coarse augmented images. The Generator generates coarse augmented images that reflect these novel variations, thereby enriching the training data and laying the groundwork for improved model ability.

In the baseline method outlined in Section 3.2.2, we input the fitted SMPL pose θ to transform the canonical human 3D Gaussians \mathcal{G}_c into observation 3D Gaussians \mathcal{G}_o for rendering. By adjusting the SMPL pose to create a new one, we can generate a human 3D Gaussian in a different observation pose. If the body pose is defined by n parameters ($\theta \in \mathbb{R}^n$), each parameter influences the spatial configuration of body parts [42]. Using the fitted SMPL Pose θ as a reference, increasing or decreasing these parameters results in corresponding changes in the observation 3D Gaussians. We associate each parameter fluctuation $\Delta\theta_i$ with a Gaussian distribution $N_i(\mu, \Sigma)$ for sampling. Larger sampled values yield greater differences between the generated \mathcal{G}_{novel} and the original \mathcal{G}_o for the respective body parts. This sampling process allows us to obtain multiple \mathcal{G}_{novel} s, which can then be used to render images I_c s of diverse human poses using Gaussian rendering techniques [23].

Similarly, for camera pose π , we can render \mathcal{G}_{novel} from views different from the original one π . We associate Gaussian distributions with the camera’s angle, distance parameters, to sample adjustments to these parameters, obtaining $\Delta\pi$, thereby obtaining different rendering viewpoints.

3.2.4 Data Construction. Using the aforementioned Generator, we create new images I_c from an original sample (consisting of a GT frame I , its fitted SMPL pose θ , and camera pose π). This is achieved by generating a new SMPL pose $\theta + \Delta\theta$ and adjusted camera parameters $\pi + \Delta\pi$. However, the resulting images are often coarse due to the limitations of the basic reconstruction model,

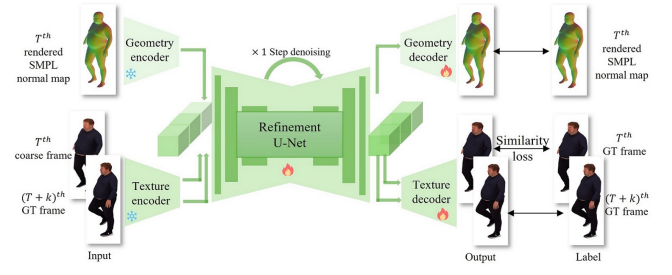


Figure 4: Refiner module. We take the refinement of the coarse frame as a single-step denoising process by treating it as a noisy image and using the GT frame as the original image, while we utilize the corresponding SMPL as geometry conditions for the coarse frame, while the adjacent GT frame are used as texture condition. The model is trained to reconstruct the GT image.

making them not ideal for training data. To enhance the quality of these coarse images, we propose training a Refiner module. Before formally introducing the Refiner, we briefly outline the training data used for the training of the Refiner in this section for clarity.

Regarding the construction of training data, as illustrated in Figure 3, we extract the corresponding SMPL poses and camera parameters for all monocular video frames about a subject [51]. By feeding these corresponding SMPL poses and camera parameters into the trained baseline model for inference, we can obtain coarse frames that correspond one-to-one with the original monocular video frames. Meanwhile, we input the corresponding SMPL parameters into the SMPL model to obtain the SMPL meshes. By combining these three elements, we establish a triplet training set.

To collect a training sample, we select a time T and randomly pick a nearby time $T + k$. This gives us four items: the GT frame I^T and coarse frame I_c^T at time T , the GT frame I^{T+k} at time $T + k$, and the SMPL normal map I_g^T rendered from the SMPL mesh at time T .

3.2.5 Refiner. As discussed in Sections 3.2.3, the samples generated by the generator offer the baseline model new images from various poses and views for training. Supplementing these additional data and distributions helps to more comprehensively optimize the model’s training parameters. However, essentially, this kind of enhancement alone cannot provide the model with additional knowledge, which restricts further performance improvement. To address this limitation, we propose the Refinement module.

Training. Figure 4 shows the training process for the Refiner, using training samples in Section 3.2.4. Initially, two images (coarse I_c^T and GT I^{T+k}), along with a normal map I_g^T , are encoded via VAE [48] encoders \mathcal{E}_t and \mathcal{E}_g , functioning as texture and geometric encoders. This encoding generates latent features $z_c = \mathcal{E}_t(I_c^T)$, $z_t = \mathcal{E}_t(I^{T+k})$, and $z_g = \mathcal{E}_g(I_g^T)$, each with dimensions $c * h * w$, where c denotes the number of channels. These features are subsequently stacked to form a tensor with dimensions $3 * c * h * w$.

The features, derived from two modalities and two views, are input into a U-Net [64], which contains self-attention layers that can facilitate interaction among the three-source features. Initially, these features are reshaped into dimensions $c * (3hw)$ for processing,

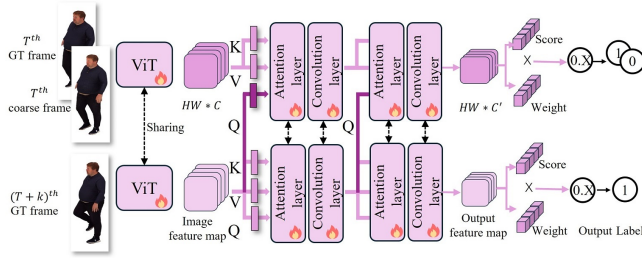


Figure 5: Examiner module. We design a dual-branch similarity examination network. It samples the coarse frame I_c^T or the GT frame I^T , and pair it with the GT frame I^{T+k} to form a tuple. In the lower branch, we directly input I^{T+k} . We extract features from I^{T+k} to serve as queries, which interact with the keys and values derived from I_c^T in the upper branch.

enabling relevant texture and geometry features from z_t and z_g to attend to the coarse image features z_c . This allows z_c to effectively absorb geometric information from z_g and texture details from z_t , compensating for the degraded information.

After passing through the U-Net, the resulting latent features, z'_c , z'_t , and z'_g , are decoded through the texture and geometric decoders to produce the refined images I'_c , I'_t , and I'_g . These images are supervised using the GT images I^T and I^{T+k} , along with the normal map I_g^T . The gradients are computed using L1, LPIPS [76], and SSIM [59] losses.

In this process, I_c^T can be interpreted as the result of adding noise ϵ to I^T . By utilizing the conditional GT image I^{T+k} and the normal map I_g^T , the training objective is to compensate for this noise ϵ , thereby achieving refinement.

Inference. As shown in Figure 2, this Refiner, following Generator, takes the coarse frame I_c as input, conditioned on its source GT frame I (whose SMPL and camera poses are θ and π), and its corresponding SMPL normal map I_g (We map the new SMPL pose $\theta + \Delta\theta$ to the SMPL mesh and render the normal map under the camera $\pi + \Delta\pi$.) to obtain the refined frame I_r .

Since the model we train adopts one-step denoising, it own fast inference speed. We directly integrated its inference into the baseline model’s one-time optimization process, enabling online refinement of the coarse frame.

3.2.6 Examiner. Using the Refiner 3.2.5, we can enhance the quality of coarse frames with a diffusion network. However, due to the inherent randomness in the diffusion model, not all refined frames may accurately match the texture of real frames in the captured monocular video. To tackle this issue and ensure the authenticity of the refined images, we introduce the Examiner module. Its primary role is to evaluate the similarity between the refined frame and the GT frame, deciding whether to accept the refined frame as pseudo-GT.

Training. As depicted in Figure 5, we start by sampling a coarse frame I_c^T and a GT frame I^{T+k} from our constructed dataset 3.2.4. These frames are then processed through Vision Transformer (ViT [6]) to extract image features, denoted as $f_c = V(I_c^T)$ and $f_k = V(I^{T+k})$. $f_c, f_k \in \mathbb{R}^{C \times (HW)}$, where (HW) is the number of spatial patches.

In the lower branch, f_k is directly processed through the attention layer [58]. This involves three linear layers to generate $K(f_k)$, $Q(f_k)$, and $V(f_k)$. An attention operation is then performed, denoted as $Attn_1(K(f_k), Q(f_k), V(f_k))$, during which we record $Q(f_k)$. In contrast, the processing of f_c is slightly different. We pass f_c through the same attention layer but only derive $K(f_c)$ and $V(f_c)$ via linear layers. They are combined with the recorded $Q(f_k)$ to execute the attention operation $Attn_1(K(f_c), V(f_c), Q(f_k))$.

This operation uses the features f_c as both the key and the value, while f_k acts as the query. This configuration is designed to examine the semantic similarity between different channels in the feature map [2, 13, 26]. Here, we use the real image semantics as a reference to emphasize those genuine semantic features in f_c related to the real image.

The output from the attention layer is reshaped to $C * H * W$ dimensions, followed by a convolution layer to squeeze the channels, promoting semantic interaction [13]. This process integrates detailed semantics, resulting in f_c^1 and $f_k^1 \in \mathbb{R}^{HW \times C^1}$. They are passed and processed through successive blocks in the same manner, as shown in Figure 5.

Ultimately, we obtain f_c^n and $f_k^n \in \mathbb{R}^{HW \times C^n}$. Each is processed through two learnable MLPs to yield f_c^s and $f_c^w \in \mathbb{R}^{HW}$, assigning scores and weights to patches. They are aggregated into the final score via weighted average. As shown in Figure 5, for the branch with I^{T+k} as the sole input, the expected training output similarity score is 1. Conversely, for the interaction between I_c^T and I^{T+k} , the expected score is 0. Moreover, during training, we not only sample I_c^T into the interaction branch but also real frame I^T with equal probability to compute similarity against I^{T+k} , where the expected output score is 1.

Inference. It can refer to Figure 2. In practical use, we obtain two refined images I_r s from an original sample (I, θ, π) via the Generator and Refiner. Both of them will be compared to I by the Examiner to calculate similarity, and we take the one with the higher similarity as the pseudo GT and discard the other one. This inference is also integrated into the baseline model’s one-time optimization.

4 Experiments

Datasets and Evaluation Metrics. To compare our method with existing methods, we follow the protocols established by previous work, ExAvatar [38]. We adopt the open monocular video dataset, Xhuman [51], focusing on subjects 00028, 00034, and 00087, alongside the NeuMan [21] dataset, maintaining the same train/test splits as in prior work. For training our Refiner and Examiner, we constructed our dataset using the Xhuman dataset [51], which includes 20 human subjects. We excluded the aforementioned three subjects and used the remaining 17 for our training. To assess the quality of our reconstruction, we adopt evaluation metrics from ExAvatar. Specifically, we computed PSNR, SSIM [59], and LPIPS [76] for our results in comparison to GT. More details of datasets, implementation and more experiments can be found in the **supplementary materials**.

Table 1: Comparisons of 3D human avatars on the test set of X-Humans dataset. Methods with * use additional depth maps for the training.

Methods	00028			00034			00087		
	PSNR \uparrow	SSIM \uparrow	LPIPS \downarrow	PSNR \uparrow	SSIM \uparrow	LPIPS \downarrow	PSNR \uparrow	SSIM \uparrow	LPIPS \downarrow
X-Avatar* [51]	28.57	0.976	0.026	28.05	0.965	0.035	30.89	0.970	0.030
ExAvatar [38]	30.58	0.981	0.018	28.75	0.966	0.029	32.01	0.972	0.025
Ours	33.04	0.985	0.014	29.87	0.968	0.026	32.82	0.974	0.023

Table 2: Comparisons on the test set of NeuMan.

Methods	PSNR \uparrow	SSIM \uparrow	LPIPS \downarrow
HumanNeRF [61]	27.06	0.967	0.019
InstantAvatar [19]	28.47	0.972	0.028
NeuMan [19]	29.32	0.972	0.014
Vid2Avatar [9]	30.70	0.980	0.014
3DGS-Avatar [44]	28.99	0.974	0.016
GaussianAvatar [14]	29.94	0.980	0.012
PGHM [43]	31.85	0.987	0.017
EVA [12]	32.02	0.982	0.015
Vid2Avatar-Pro [10]	32.71	0.983	0.012
MonoCloth [10]	33.53	0.986	0.012
PriorAvatar [20]	33.64	0.984	0.011
ExAvatar [38]	34.80	0.984	0.009
Ours	35.42	0.987	0.009

Table 3: Module ablation study. Over the baseline, we gradually add the three proposed modules, and the model’s performance improves progressively as we incorporate each new module.

Methods	00028		
	PSNR \uparrow	SSIM \uparrow	LPIPS \downarrow
Baseline	30.5842	0.9814	0.0181
+ Generator	31.2905	0.9825	0.0170
+ Generator&Refiner	32.6586	0.9847	0.0146
+ Generator&Refiner&Examiner	33.0412	0.9851	0.0143
00034			
Baseline	28.7533	0.9659	0.0292
+ Generator	28.9654	0.9665	0.0280
+ Generator&Refiner	29.6413	0.9678	0.0263
+ Generator&Refiner&Examiner	29.8745	0.9681	0.0261

4.1 Quantitative Comparison with SOTA methods

In Tables 1 and 2, our method outperforms existing approaches on both X-Humans and NeuMan datasets. Specifically, on X-Humans, for the subject 00028, our method outperforms the baseline ExAvatar by 2.46 in PSNR and 0.004 in SSIM. On NeuMan, our method yields a PSNR improvement of 0.62. These improvements stem from

Table 4: More ablation study about Refiner. Based on the Generator, we explore the impact of different conditions in the Refiner on the final results. Without any guiding conditions, the refinement leads to a slight decrease. However, as we add texture and geometry conditions, the results gradually improve.

Methods	00028		
	PSNR \uparrow	SSIM \uparrow	LPIPS \downarrow
Coarse image Generation	31.2905	0.9825	0.0170
+ Refinement (Without condition)	30.9897	0.9818	0.0172
+ Refinement (Only Tex. condition)	32.1369	0.9841	0.0155
+ Refinement (Tex.&Geo. condition)	32.6586	0.9847	0.0146
00034			
Coarse image Generation	28.9654	0.9665	0.0280
+ Refinement (Without condition)	28.9375	0.9663	0.0283
+ Refinement (Only Tex. condition)	29.4364	0.9674	0.0266
+ Refinement (Tex.&Geo. condition)	29.6413	0.9678	0.0263

our tri-module augmentation framework, which enriches training data diversity via the Generator, refines synthetic-real consistency through the Refiner, and ensures high-quality samples via the Examiner, collectively boosting reconstruction results. **The results of other methods in the tables mainly come from ExAvatar [38]. We obtain their respective results from works [10, 20, 22, 43]. Moreover, we reproduce EVA [12] for the results.**

4.2 Quantitative Ablation Study

Module Ablation. We perform ablation studies on our modules (Generator, Refiner, Examiner) in Table 3, observing consistent gains with each addition. The reason lies in that the Generator synthesizes diverse unseen images via Gaussian-guided pose/camera perturbations. Supplementing these additional data and distributions helps more comprehensively optimize the model’s training parameters. The Refiner uses diffusion networks to refine the Generator’s coarse frames, boosting image quality, thus improving reconstruction results. The Examiner filters refined frames by GT similarity, retaining only high-consistency pseudo-GT.

Refiner Ablation. We ablate the Refiner’s conditioning factors in Table 4. Unconditional refinement degrades performance, as it can randomly alter critical details, as illustrated in Figure 8. In contrast, incorporating texture and geometry conditions leads to consistent performance improvements. Texture conditions ensure

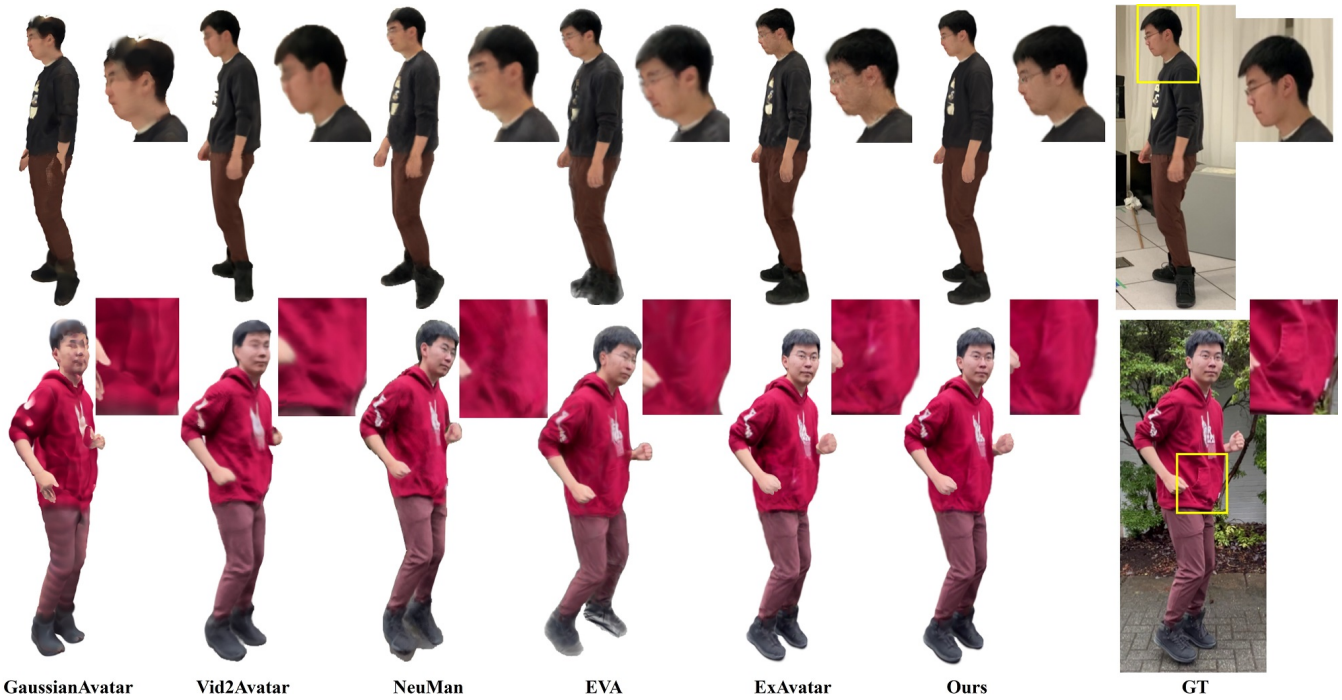


Figure 6: Visual comparison with SOTA methods on Neuman. Compared to current methods, our approach can achieve better reconstruction performance, such as reducing artifacts on side profiles of faces and providing clearer details of clothing pockets.

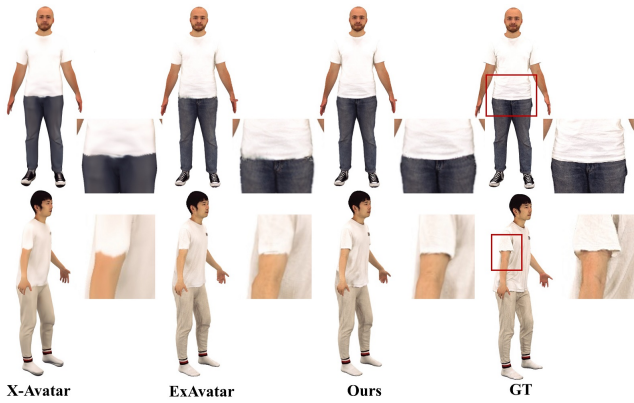


Figure 7: Visual comparison with SOTA methods on X-Human. Compared to these existing approaches, our method delivers superior reconstruction performance, particularly in capturing details like clothing wrinkles and edges.

detail similarity to the original frame, while geometry conditions maintain geometric correctness. This is visually demonstrated in Figures 8 and 10.

4.3 Visualization

Comparison with SOTA Methods. In Figures 1, 6, and 7, we demonstrate that our method outperforms existing approaches in detail reconstruction, particularly for clothing wrinkles and edges.

This superiority arises from our framework’s supplement of high-quality data: the Generator enhances training diversity with varied fabric textures and wrinkle configurations, the Refiner boosts texture precision, and the Examiner ensures data authenticity. Together, these components equip the model with richer cues for capturing clothing nuances, unlike baseline methods constrained by limited training data. **Notably, some works [10, 20, 22, 43] have not open-sourced their codes.**

Visual Ablation. Figures 8 and 10 showcase the Refiner’s effectiveness in refining coarse images. We find that incorporating texture and geometric conditions enhances performance: texture condition reduces the model’s tendency to produce artifacts, like the pattern in the clothes, while adding geometric conditions improves the model’s ability to enhance human geometric details, like the human fingers. The reason is that during the use of the diffusion model, the model can randomly introduce some false illusions. However, by adding texture semantic constraints of the neighborhood frames and geometric constraints, the direction of model diffusion can be effectively corrected.

Examiner Visualization. In Figure 9, we present the similarity density functions of the Examiner’s outputs for various image types. The figure shows the Examiner’s ability to differentiate between high-quality refined frames (closely matching GT) and low-quality ones (affected by false hallucination, like the examples shown in Figure 8). This ability is vital because the Refiner, while enhancing frame quality through diffusion, can introduce randomness that leads to semantics-misaligned outputs. Without the Examiner, these

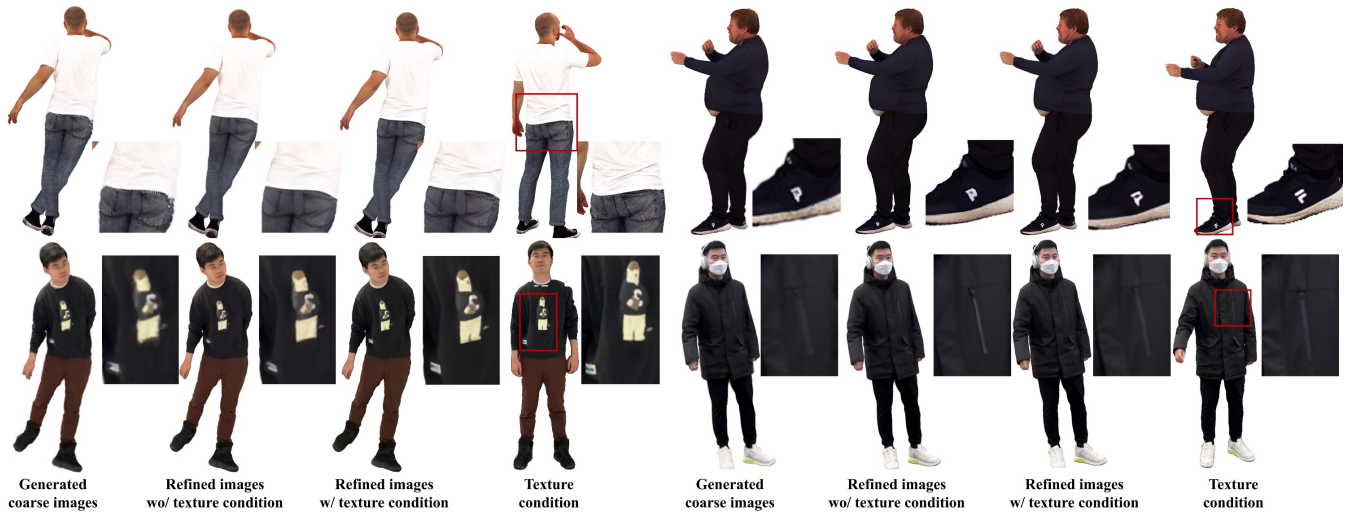


Figure 8: Visual ablation of Refiner. We show the refinement effects of the Refiner module before and after incorporating texture conditions, highlighting a notable improvement in image quality. The introduction of texture conditions enhances details like wrinkles and patterns on clothing in the left two groups. In contrast, without these conditions, the Refiner would incorrectly enhance certain features, leading to false hallucination, as shown in the right two groups with shoe patterns and clothing designs.

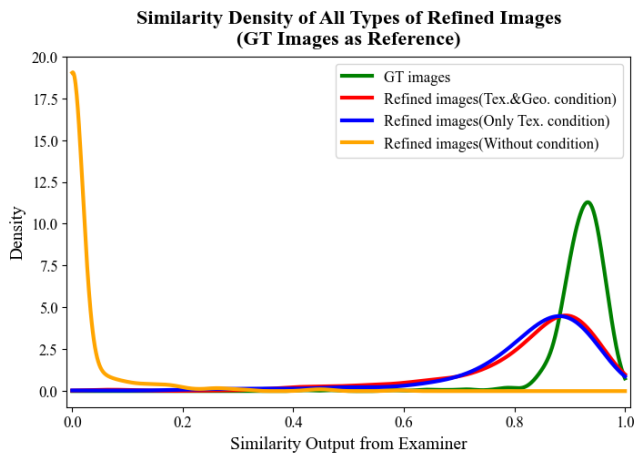


Figure 9: Visualization about Examiner. It is found that Examiner can distinguish between different refined images. When GT images are input, the similarity values approach 1, while for images refined without conditions, they approach 0. Applying conditions like texture and geometry improves the authenticity of refined images, though some instances of low authenticity still occur.

flawed samples could contaminate training. By filtering out low-similarity frames, the Examiner ensures that more authentic refined images are retained. Due to the geometry condition’s ability to assist with fine-grained geometric details (Figure 10), it can further enhance similarity.

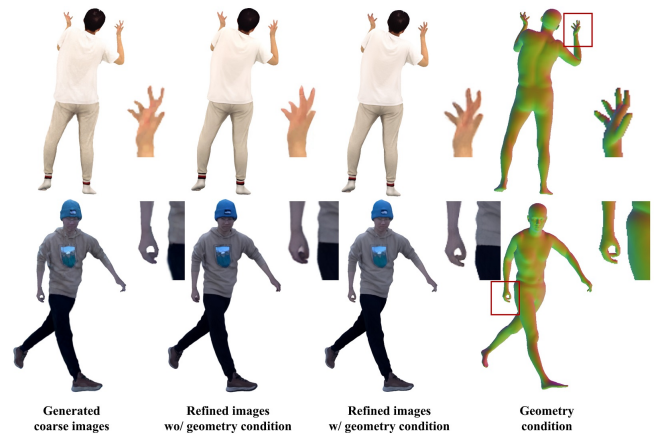


Figure 10: Visual ablation about the geometry condition in Refiner. It is observed that introducing geometric conditions in the Refiner module enhances the improvement of human geometric quality, such as the details of the fingers.

5 Conclusion

In this paper, we presented TrioMan, a tri-module augmented framework that effectively addresses the data scarcity and viewpoint limitations inherent in monocular avatar reconstruction. By synergizing a distribution-perturbed Generator, a one-step diffusion-based Refiner, and a dual-branch attention Examiner, our approach systematically enriches training diversity while ensuring the photorealism and reliability of synthetic samples. Extensive experiments on the X-Humans and NeuMan benchmarks demonstrate that TrioMan achieves state-of-the-art performance, greatly improving pose generalization and rendering fidelity. Ultimately, our work provides a robust solution for recovering high-fidelity, subject-specific 3D

avatars from limited monocular input, paving the way for more accessible and immersive digital human applications.

References

- [1] Timur Bagautdinov, Chenglei Wu, Tomas Simon, Fabián Prada, Takaaki Shiratori, Shih-En Wei, Weipeng Xu, Yaser Sheikh, and Jason Saragih. 2021. Driving-signal aware full-body avatars. *ACM Trans. Graph.* 40, 4, Article 143 (July 2021), 17 pages. doi:10.1145/3450626.3459850
- [2] Dongliang Chang, Yifeng Ding, Jiyang Xie, Ayan Kumar Bhunia, and Yi Zhe Song. 2020. The Devil is in the Channels: Mutual-Channel Loss for Fine-Grained Image Classification. *IEEE Transactions on Image Processing* PP, 99 (2020), 1–1.
- [3] Yushuo Chen, Zerong Zheng, Zhe Li, Chao Xu, and Yebin Liu. 2024. MeshAvatar: Learning High-quality Triangular Human Avatars from Multi-view Videos. arXiv:2407.08414 [cs.CV]
- [4] Chong Cheng, Gaochao Song, Yiyang Yao, Qinzhen Zhou, Gangjian Zhang, and Hao Wang. 2025. Graph-Guided Scene Reconstruction from Images with 3D Gaussian Splatting. arXiv:2502.17377 [cs.CV] <https://arxiv.org/abs/2502.17377>
- [5] Wei Cheng, Ruixiang Chen, Siming Fan, Wanqi Yin, Keyu Chen, Zhongang Cai, Jingbo Wang, Yang Gao, Zhengming Yu, Zhengyu Lin, et al. 2023. Dna-rendering: A diverse neural actor repository for high-fidelity human-centric rendering. In *Proceedings of the IEEE/CVF International Conference on Computer Vision*. 19982–19993.
- [6] Alexey Dosovitskiy, Lucas Beyer, Alexander Kolesnikov, Dirk Weissenborn, Xi-aohua Zhai, Thomas Unterthiner, Mostafa Dehghani, Matthias Minderer, Georg Heigold, Sylvain Gelly, et al. 2020. An image is worth 16x16 words: Transformers for image recognition at scale. *arXiv preprint arXiv:2010.11929* (2020).
- [7] Yuanxing Duan, Fangyin Wei, Qiyu Dai, Yuhang He, Wenzheng Chen, and Baoquan Chen. 2024. 4d-rotor gaussian splatting: towards efficient novel view synthesis for dynamic scenes. In *ACM SIGGRAPH 2024 Conference Papers*. 1–11.
- [8] Yao Feng, Jinlong Yang, Marc Pollefeys, Michael J. Black, and Timo Bolkart. 2022. Capturing and Animation of Body and Clothing from Monocular Video. In *SIGGRAPH Asia 2022 Conference Papers* (Daegu, Republic of Korea) (SA '22). Association for Computing Machinery, New York, NY, USA, Article 45, 9 pages. doi:10.1145/3550469.3555423
- [9] Chen Guo, Tianjian Jiang, Xu Chen, Jie Song, and Otmar Hilliges. 2023. Vid2Avatar: 3D Avatar Reconstruction from Videos in the Wild via Self-supervised Scene Decomposition. In *Proceedings of the IEEE/CVF Conference on Computer Vision and Pattern Recognition (CVPR)*.
- [10] Chen Guo, Junxuan Li, Yash Kant, Yaser Sheikh, Shunsuke Saito, and Chen Cao. 2022. Vid2avatar-pro: Authentic avatar from videos in the wild via universal prior. In *Proceedings of the Computer Vision and Pattern Recognition Conference*. 5559–5570.
- [11] Jonathan Ho, Ajay Jain, and Pieter Abbeel. 2020. Denoising Diffusion Probabilistic Models. arXiv:2006.11239 [cs.LG]
- [12] Hezhen Hu, Zhiwen Fan, Tianhao Wu, Yihan Xi, Seoyoung Lee, Georgios Pavlakos, and Zhangyang Wang. 2024. Expressive Gaussian Human Avatars from Monocular RGB Video. In *NeurIPS*.
- [13] Jie Hu, Li Shen, and Gang Sun. 2018. Squeeze-and-excitation networks. In *Proceedings of the IEEE conference on computer vision and pattern recognition*. 7132–7141.
- [14] Liangxiao Hu, Hongwen Zhang, Yuxiang Zhang, Boyao Zhou, Boning Liu, Shengping Zhang, and Liqiang Nie. 2024. GaussianAvatar: Towards Realistic Human Avatar Modeling from a Single Video via Animatable 3D Gaussians. In *IEEE/CVF Conference on Computer Vision and Pattern Recognition (CVPR)*.
- [15] Liangxiao Hu, Hongwen Zhang, Yuxiang Zhang, Boyao Zhou, Boning Liu, Shengping Zhang, and Liqiang Nie. 2024. Gaussianavatar: Towards realistic human avatar modeling from a single video via animatable 3d gaussians. In *Proceedings of the IEEE/CVF conference on computer vision and pattern recognition*. 634–644.
- [16] Shoukang Hu, Tao Hu, and Ziwei Liu. 2024. Gauhuman: Articulated gaussian splatting from monocular human videos. In *Proceedings of the IEEE/CVF Conference on Computer Vision and Pattern Recognition*. 20418–20431.
- [17] Yi-Hua Huang, Yang-Tian Sun, Ziyi Yang, Xiaoyang Lyu, Yan-Pei Cao, and Xiaojuan Qi. 2024. Sc-gs: Sparse-controlled gaussian splatting for editable dynamic scenes. In *Proceedings of the IEEE/CVF conference on computer vision and pattern recognition*. 4220–4230.
- [18] Boyi Jiang, Yang Hong, Hujun Bao, and Juyong Zhang. 2022. Selfrecon: Self reconstruction your digital avatar from monocular video. In *Proceedings of the IEEE/CVF Conference on Computer Vision and Pattern Recognition*. 5605–5615.
- [19] Tianjian Jiang, Xu Chen, Jie Song, and Otmar Hilliges. 2023. InstantAvatar: Learning Avatars from Monocular Video in 60 Seconds. (June 2023).
- [20] Tianjian Jiang, Hsuan-I Ho, Manuel Kaufmann, and Jie Song. 2025. PriorAvatar: Efficient and Robust Avatar Creation from Monocular Video Using Learned Priors. In *Proceedings of the SIGGRAPH Asia 2025 Conference Papers* (SA Conference Papers '25). Association for Computing Machinery, New York, NY, USA, Article 31, 10 pages. doi:10.1145/3757377.3763978
- [21] Wei Jiang, Kwang Moo Yi, Golnoosh Samei, Oncel Tuzel, and Anurag Ranjan. 2022. NeuMan: Neural Human Radiance Field from a Single Video. In *Proceedings of the European conference on computer vision (ECCV)*.
- [22] Daisheng Jin and Ying He. 2026. MonoCloth: Reconstruction and Animation of Cloth-Decoupled Human Avatars from Monocular Videos. In *Proceedings of the AAAI Conference on Artificial Intelligence*, Vol. 40. 5503–5511.
- [23] Bernhard Kerbl, Georgios Kopanas, Thomas Leimkuehler, and George Drettakis. 2023. 3D Gaussian Splatting for Real-Time Radiance Field Rendering. *ACM Trans. Graph.* 42, 4, Article 139 (jul 2023), 14 pages. doi:10.1145/3592433
- [24] Muhammed Kocabas, Jen-Hao Rick Chang, James Gabriel, Oncel Tuzel, and Anurag Ranjan. 2024. Hugs: Human gaussian splats. In *Proceedings of the IEEE/CVF conference on computer vision and pattern recognition*. 505–515.
- [25] Muhammed Kocabas, Jen-Hao Rick Chang, James Gabriel, Oncel Tuzel, and Anurag Ranjan. 2024. Hugs: Human gaussian splats. In *Proceedings of the IEEE/CVF conference on computer vision and pattern recognition*. 505–515.
- [26] SuBeen Lee, WonJun Moon, Hyun Seok Seong, and Jae-Pil Heo. 2024. Task-oriented channel attention for fine-grained few-shot classification. *IEEE Transactions on Pattern Analysis and Machine Intelligence* (2024).
- [27] Jiahui Lei, Yufu Wang, Georgios Pavlakos, Lingjie Liu, and Kostas Daniilidis. 2024. Gart: Gaussian articulated template models. In *Proceedings of the IEEE/CVF conference on computer vision and pattern recognition*. 19876–19887.
- [28] Mingwei Li, Jiachen Tao, Zongxin Yang, and Yi Yang. 2023. Human101: Training 100+FPS Human Gaussians in 100s from 1 View. arXiv:2312.15258 [cs.CV]
- [29] Mengtian Li, Shengxiang Yao, Zhifeng Xie, and Keyu Chen. 2024. Gaussian-body: Clothed human reconstruction via 3d gaussian splatting. *arXiv preprint arXiv:2401.09720* (2024).
- [30] Zhan Li, Zhang Chen, Zhong Li, and Yi Xu. 2024. Spacetime gaussian feature splatting for real-time dynamic view synthesis. In *Proceedings of the IEEE/CVF Conference on Computer Vision and Pattern Recognition*. 8508–8520.
- [31] Shanchuan Lin, Anran Wang, and Xiao Yang. 2024. Sdxl-lightning: Progressive adversarial diffusion distillation. *arXiv preprint arXiv:2402.13929* (2024).
- [32] Youtian Lin, Zuozhuo Dai, Siyu Zhu, and Yao Yao. 2024. Gaussian-flow: 4d reconstruction with dynamic 3d gaussian particle. In *Proceedings of the IEEE/CVF Conference on Computer Vision and Pattern Recognition*. 21136–21145.
- [33] Fangfu Liu, Wenqiang Sun, Hanyang Wang, Yikai Wang, Haowen Sun, Junliang Ye, Jun Zhang, and Yueqi Duan. 2024. Reconx: Reconstruct any scene from sparse views with video diffusion model. *arXiv preprint arXiv:2408.16767* (2024).
- [34] Xinqi Liu and Chenming Wu. 2025. VGA: Reconstructing Vivid 3D Gaussian Avatars from Monocular Videos. In *International Conference on Computational Visual Media*. Springer, 172–193.
- [35] Xian Liu, Xiaohang Zhan, Jiaxiang Tang, Ying Shan, Gang Zeng, Dahua Lin, Xihui Liu, and Ziwei Liu. 2024. Humangaussian: Text-driven 3d human generation with gaussian splatting. In *Proceedings of the IEEE/CVF Conference on Computer Vision and Pattern Recognition*. 6646–6657.
- [36] Matthew Loper, Naureen Mahmood, Javier Romero, Gerard Pons-Moll, and Michael J Black. 2023. SMPL: A skinned multi-person linear model. In *Seminal Graphics Papers: Pushing the Boundaries, Volume 2*. 851–866.
- [37] Ben Mildenhall, Pratul P. Srinivasan, Matthew Tancik, Jonathan T. Barron, Ravi Ramamoorthi, and Ren Ng. 2020. NeRF: Representing Scenes as Neural Radiance Fields for View Synthesis. In *ECCV*.
- [38] Gyeongsik Moon, Takaaki Shiratori, and Shunsuke Saito. 2024. Expressive Whole-body 3D Gaussian Avatar. In *ECCV*.
- [39] Gyeongsik Moon, Takaaki Shiratori, and Shunsuke Saito. 2024. Expressive whole-body 3d gaussian avatar. In *European Conference on Computer Vision*. Springer, 19–35.
- [40] Arthur Moreau, Jifei Song, Helisa Dharmo, Richard Shaw, Yiren Zhou, and Eduardo Pérez-Pellitero. 2024. Human gaussian splatting: Real-time rendering of animatable avatars. In *Proceedings of the IEEE/CVF conference on computer vision and pattern recognition*. 788–798.
- [41] Jongmin Park, Minh-Quan Viet Bui, Juan Luis Gonzalez Bello, Jaeho Moon, Jihyong Oh, and Munchurl Kim. 2025. Splines: Robust motion-adaptive spline for real-time dynamic 3d gaussians from monocular video. In *Proceedings of the Computer Vision and Pattern Recognition Conference*. 26866–26875.
- [42] Georgios Pavlakos, Vasileios Choutas, Nima Ghorbani, Timo Bolkart, Ahmed A. A. Osman, Dimitrios Tzionas, and Michael J. Black. 2019. Expressive Body Capture: 3D Hands, Face, and Body from a Single Image. In *Proceedings IEEE Conf. on Computer Vision and Pattern Recognition (CVPR)*.
- [43] Cheng Peng, Jingxiang Sun, Yushuo Chen, Zhaoqi Su, Zhuo Su, and Yebin Liu. 2025. Parametric Gaussian Human Model: Generalizable Prior for Efficient and Realistic Human Avatar Modeling. *arXiv preprint arXiv:2506.06645* (2025).
- [44] Zhiyin Qian, Shaofei Wang, Marko Mihajlovic, Andreas Geiger, and Siyu Tang. 2024. 3DGS-Avatar: Animatable Avatars via Deformable 3D Gaussian Splatting (2024).
- [45] Lingteng Qiu, Xiaodong Gu, Peihao Li, Qi Zuo, Weichao Shen, Junfei Zhang, Kejie Qiu, Weihao Yuan, Guanying Chen, Zilong Dong, et al. 2025. Lhm: Large animatable human reconstruction model from a single image in seconds. *arXiv preprint arXiv:2503.10625* (2025).
- [46] Lingteng Qiu, Peihao Li, Qi Zuo, Xiaodong Gu, Yuan Dong, Weihao Yuan, Siyu Zhu, Xiaoguang Han, Guanying Chen, and Zilong Dong. 2025. PF-LHM: 3D Animatable Avatar Reconstruction from Pose-free Articulated Human Images.

- arXiv preprint arXiv:2506.13766* (2025).
- [47] Javier Romero, Dimitrios Tzionas, and Michael J Black. 2022. Embodied hands: Modeling and capturing hands and bodies together. *arXiv preprint arXiv:2201.02610* (2022).
- [48] Axel Sauer, Dominik Lorenz, Andreas Blattmann, and Robin Rombach. 2024. Adversarial Diffusion Distillation. In *Computer Vision – ECCV 2024: 18th European Conference, Milan, Italy, September 29–October 4, 2024, Proceedings, Part LXXXVI* (Milan, Italy). Springer-Verlag, Berlin, Heidelberg, 87–103. doi:10.1007/978-3-031-73016-0_6
- [49] Zhijing Shao, Zhaolong Wang, Zhuang Li, Duotun Wang, Xiangru Lin, Yu Zhang, Mingming Fan, and Zeyu Wang. 2024. Splattingavatar: Realistic real-time human avatars with mesh-embedded gaussian splatting. In *Proceedings of the IEEE/CVF Conference on Computer Vision and Pattern Recognition*. 1606–1616.
- [50] Zhijing Shao, Zhaolong Wang, Zhuang Li, Duotun Wang, Xiangru Lin, Yu Zhang, Mingming Fan, and Zeyu Wang. 2024. Splattingavatar: Realistic real-time human avatars with mesh-embedded gaussian splatting. In *Proceedings of the IEEE/CVF Conference on Computer Vision and Pattern Recognition*. 1606–1616.
- [51] Kaiyue Shen, Chen Guo, Manuel Kaufmann, Juan Zarate, Julien Valentin, Jie Song, and Otmar Hilliges. 2023. X-Avatar: Expressive Human Avatars. *Computer Vision and Pattern Recognition (CVPR)*.
- [52] Jian Shu, Nanjie Yao, Gangjian Zhang, Junlong Ren, Yu Feng, and Hao Wang. 2025. FastAnimate: Towards Learnable Template Construction and Pose Deformation for Fast 3D Human Avatar Animation. arXiv:2512.01444 [cs.CV] <https://arxiv.org/abs/2512.01444>
- [53] Geonhee Sim and Gyeongsik Moon. 2025. PERSONA: Personalized Whole-Body 3D Avatar with Pose-Driven Deformations from a Single Image. In *Proceedings of the IEEE/CVF International Conference on Computer Vision*. 12670–12680.
- [54] Shih-Yang Su, Timur Bagautdinov, and Helge Rhodin. 2023. Npc: Neural point characters from video. In *Proceedings of the IEEE/CVF International conference on computer vision*. 14795–14805.
- [55] Shih-Yang Su, Frank Yu, Michael Zollhöfer, and Helge Rhodin. 2021. A-nerf: Articulated neural radiance fields for learning human shape, appearance, and pose. *Advances in neural information processing systems* 34 (2021), 12278–12291.
- [56] David Svitov, Pietro Morerio, Lourdes Agapito, and Alessio Del Bue. 2024. Haha: Highly articulated gaussian human avatars with textured mesh prior. In *Proceedings of the Asian Conference on Computer Vision*. 4051–4068.
- [57] Gusi Te, Xiu Li, Xiao Li, Jinglu Wang, Wei Hu, and Yan Lu. 2022. Neural capture of animatable 3d human from monocular video. In *European Conference on Computer Vision*. Springer, 275–291.
- [58] Ashish Vaswani, Noam Shazeer, Niki Parmar, Jakob Uszkoreit, Llion Jones, Aidan N Gomez, Lukasz Kaiser, and Illia Polosukhin. 2017. Attention is all you need. *Advances in neural information processing systems* 30 (2017).
- [59] Zhou Wang and Alan Conrad Bovik. 2006. Modern image quality assessment. (2006).
- [60] Jing Wen, Xiaoming Zhao, Zhongzheng Ren, Alexander G Schwing, and Shenlong Wang. 2024. Gomavatar: Efficient animatable human modeling from monocular video using gaussians-on-mesh. In *Proceedings of the IEEE/CVF Conference on Computer Vision and Pattern Recognition*. 2059–2069.
- [61] Chung-Yi Weng, Brian Curless, Pratul P. Srinivasan, Jonathan T. Barron, and Ira Kemelmacher-Shlizerman. 2022. HumanNeRF: Free-Viewpoint Rendering of Moving People From Monocular Video. In *Proceedings of the IEEE/CVF Conference on Computer Vision and Pattern Recognition (CVPR)*. 16210–16220.
- [62] Chung-Yi Weng, Brian Curless, Pratul P Srinivasan, Jonathan T Barron, and Ira Kemelmacher-Shlizerman. 2022. Humannerf: Free-viewpoint rendering of moving people from monocular video. In *Proceedings of the IEEE/CVF conference on computer vision and pattern Recognition*. 16210–16220.
- [63] Guanjun Wu, Taoran Yi, Jiemin Fang, Lingxi Xie, Xiaopeng Zhang, Wei Wei, Wenyu Liu, Qi Tian, and Xinggang Wang. 2024. 4d gaussian splatting for real-time dynamic scene rendering. In *Proceedings of the IEEE/CVF conference on computer vision and pattern recognition*. 20310–20320.
- [64] Jay Zhangjie Wu, Yuxuan Zhang, Haitthem Turki, Xuanchi Ren, Jun Gao, Mike Zheng Shou, Sanja Fidler, Zan Gojic, and Huan Ling. 2025. DIFIX3D+: Improving 3D Reconstructions with Single-Step Diffusion Models. In *Proceedings of the Computer Vision and Pattern Recognition Conference*. 26024–26035.
- [65] Zhangyang Xiong, Chenghong Li, Kenkun Liu, Hongjie Liao, Jianqiao Hu, Junyi Zhu, Shuliang Ning, Lingteng Qiu, Chongjie Wang, Shijie Wang, et al. 2024. MVHumanNet: A Large-scale Dataset of Multi-view Daily Dressing Human Captures. In *Proceedings of the IEEE/CVF Conference on Computer Vision and Pattern Recognition*. 19801–19811.
- [66] Jiawei Xu, Zexin Fan, Jian Yang, and Jin Xie. 2024. Grid4d: 4d decomposed hash encoding for high-fidelity dynamic gaussian splatting. *Advances in Neural Information Processing Systems* 37 (2024), 123787–123811.
- [67] Ziyi Yang, Xinyu Gao, Wen Zhou, Shaohui Jiao, Yuqing Zhang, and Xiaogang Jin. 2024. Deformable 3d gaussians for high-fidelity monocular dynamic scene reconstruction. In *Proceedings of the IEEE/CVF conference on computer vision and pattern recognition*. 20331–20341.
- [68] Zeyu Yang, Hongye Yang, Zijie Pan, and Li Zhang. 2023. Real-time photorealistic dynamic scene representation and rendering with 4d gaussian splatting. *arXiv preprint arXiv:2310.10642* (2023).
- [69] Nanjie Yao, Gangjian Zhang, Wenhao Shen, Jian Shu, Yu Feng, and Hao Wang. 2026. MultiGO++: Monocular 3D Clothed Human Reconstruction via Geometry-Texture Collaboration. *arXiv preprint arXiv:2603.04993* (2026).
- [70] Tianwei Yin, Michaël Gharbi, Richard Zhang, Eli Shechtman, Fredo Durand, William T Freeman, and Taesung Park. 2024. One-step diffusion with distribution matching distillation. In *Proceedings of the IEEE/CVF conference on computer vision and pattern recognition*. 6613–6623.
- [71] Heng Yu, Joel Julin, Zoltán Á Milacski, Koichiro Niinuma, and László A Jeni. 2024. Cogs: Controllable gaussian splatting. In *Proceedings of the IEEE/CVF Conference on Computer Vision and Pattern Recognition*. 21624–21633.
- [72] Wangbo Yu, Jinbo Xing, Li Yuan, Wenbo Hu, Xiaoyu Li, Zhipeng Huang, Xiangjun Gao, Tien-Tsin Wong, Ying Shan, and Yonghong Tian. 2024. Viewcrafter: Taming video diffusion models for high-fidelity novel view synthesis. *arXiv preprint arXiv:2409.02048* (2024).
- [73] Zhengming Yu, Wei Cheng, Xian Liu, Wayne Wu, and Kwan-Yee Lin. 2023. Monohuman: Animatable human neural field from monocular video. In *Proceedings of the IEEE/CVF Conference on Computer Vision and Pattern Recognition*. 16943–16953.
- [74] Gangjian Zhang, Jian Shu, Nanjie Yao, and Hao Wang. 2025. SAT: Supervisor Regularization and Animation Augmentation for Two-process Monocular Texture 3D Human Reconstruction. In *Proceedings of the 33rd ACM International Conference on Multimedia (Dublin, Ireland) (MM '25)*. Association for Computing Machinery, New York, NY, USA, 10563–10572. doi:10.1145/3746027.3755774
- [75] Gangjian Zhang, Nanjie Yao, Shunsi Zhang, Hanfeng Zhao, Guoliang Pang, Jian Shu, and Hao Wang. 2025. Multigo: Towards multi-level geometry learning for monocular 3d textured human reconstruction. In *Proceedings of the Computer Vision and Pattern Recognition Conference*. 338–347.
- [76] Richard Zhang, Phillip Isola, Alexei A Efros, Eli Shechtman, and Oliver Wang. 2018. The unreasonable effectiveness of deep features as a perceptual metric. In *Proceedings of the IEEE conference on computer vision and pattern recognition*. 586–595.
- [77] Shunyuhan Zheng, Boyao Zhou, Ruizhi Shao, Boning Liu, Shengping Zhang, Liqiang Nie, and Yebin Liu. 2024. GPS-Gaussian: Generalizable Pixel-wise 3D Gaussian Splatting for Real-time Human Novel View Synthesis. In *Proceedings of the IEEE/CVF Conference on Computer Vision and Pattern Recognition (CVPR)*.
- [78] Yingji Zhong, Zhihao Li, Dave Zhenyu Chen, Lanqing Hong, and Dan Xu. 2025. Taming Video Diffusion Prior with Scene-Grounding Guidance for 3D Gaussian Splatting from Sparse Inputs. In *Proceedings of the Computer Vision and Pattern Recognition Conference*. 6133–6143.